

Cathodoluminescence microcharacterization of the defect structure of quartz

M. A. Stevens Kalceff and M. R. Phillips

Electron Microscope Facility, University of Technology, Sydney, P.O. Box 123, Broadway, New South Wales 2007, Australia

(Received 2 March 1995)

Cathodoluminescence (CL) spectroscopy has been used to investigate the irradiation-sensitive defect structure of ultrapure synthetic quartz at 295 and 80 K. CL emissions are identified with particular defect centers. Insight into the processes of defect formation and subsequent electromigration resulting from the trapped-charge-induced electric field following irradiation by a stationary continuous electron beam are presented. The CL emissions are associated with either a nonbridging oxygen hole center (NBOHC) or trapped-electron Si_3^- center (1.91 eV); NBOHC with OH precursor (1.95 eV); the radiative recombination of the self-trapped exciton (STE) in irradiation-induced amorphous SiO_2 outgrowths (2.28 eV); an extrinsic process (2.46 eV); the radiative recombination of the STE associated with the E'_1 center in $\alpha\text{-SiO}_2$ (2.72 eV); an additional component at 80 K due to the radiative recombination of the STE associated with the E'_2 center (2.69 eV); an intrinsic process (2.95 eV); and the charge-compensated substitutional aluminum center (3.12 eV).

I. INTRODUCTION

Cathodoluminescence (CL) microscopy and spectroscopy in a scanning electron microscope (SEM) are particularly suitable techniques for the high spatial resolution, high sensitivity detection of defect centers in materials.^{1,2} Recent developments in photonics technology have resulted in an increase in the application¹⁻⁵ of materials characterization using CL microanalysis. For example, following the identification of the mechanisms producing the emission bands in the CL spectrum, the migration and electrodiffusion of particular luminescent centers may be imaged with high spatial resolution using monochromatic CL microscopy. In addition, nondestructive depth resolved (nm to μm) information is available by varying the electron-beam energy and hence the interaction volume. CL microanalysis complements the defect structure information available from other luminescence spectroscopy such as photoluminescence (PL), optical-absorption spectroscopy, electron-spin-resonance, and electron paramagnetic resonance (ESR/EPR) spectroscopies.

In this investigation, CL microcharacterization has been used to investigate the irradiation sensitive defect structure of crystalline SiO_2 (quartz). The luminescence emissions are correlated with particular defect structures. In addition insight obtained from CL analysis into the processes of defect formation and subsequent electrodiffusion due to the influence of the electric field induced by trapped charges within the interaction volume^{6,7} are presented.

Silicon dioxide (SiO_2) is a semicovalent^{6,8} oxide insulator with useful physical properties that have resulted in its wide and diverse use. Some of the many applications include the use of natural SiO_2 (quartz) as a geological indicator, as the concentration of certain impurity and structural defects indicates the genesis of the quartz^{2,9,10} and hence possible associated valuable oil, gas, and mineral deposits. Synthetic SiO_2 polymorphs are also

used in optical fiber technology, laser windows, and in semiconductor and frequency control devices. The presence of impurities and structural defects may affect the device performance.^{11,12} In addition it is well recognized that the defect structure of SiO_2 is extremely sensitive to ionizing radiation.¹¹⁻¹⁴ Many SiO_2 devices are operated in radiation environments, therefore it is of fundamental importance to characterize the radiation sensitive defect structure of SiO_2 to enable optimum device design.

It has been observed that the method of SiO_2 synthesis,¹⁵ irradiation,^{16,17} mechanical stress,^{18,19} temperature change,^{20,21} and the presence of (trace amounts of) impurities^{12,13,17,20,22,23} can effect the formation of defects and/or the transformation of existing defect precursors in SiO_2 .¹⁵ Irradiation produces defects by either the trapping of an electron or hole at the site of a preexisting precursor defect. Alternatively, atomic displacements from the normal bonding (defect-free) sites can result from either knock on^{14,22} ($E_0 > 100$ keV) or radiolytic processes⁶ ($E_0 > 5$ keV) depending on the irradiation energy E_0 .¹³

ESR/EPR are powerful and widely used techniques available for the detection and identification of paramagnetic defects. ESR/EPR studies have identified three types of fundamental defects induced by the irradiation of high purity SiO_2 (see Griscom's excellent review¹³ and references therein). They are the E' center,¹⁶ the peroxy (or "superoxide"³⁵) radical,²⁴ and the nonbridging oxygen hole center (NBOHC).²⁵ Models for each defect have been proposed, based on large experimental data bases.¹³

The E' center is usually denoted ($\equiv\text{Si}\cdot$) which represents an unpaired electron (\cdot) in a dangling tetrahedral sp^3 orbital of a single silicon atom bonded to three oxygen atoms (\equiv) in the SiO_2 structure. A number of E' center variants have been identified, including the E'_1 ,²⁶ E'_2 ,¹⁶ and E'_α (Ref. 13) centers which are radiolytically formed and are believed to involve the asymmetrically related oxygen vacancy;²⁷ E'_4 (Refs. 16 and 28) and E'_β (Refs. 13 and 22) centers which are produced by the irradiation of an oxygen vacancy and stabi-

lized by hydrogen; E'_γ and E'_δ centers,¹³ and the E'_s center in the surface region, and others (see, for example, Conley *et al.*²⁹ for discussion of further E' variants). The peroxy radical is an oxygen associated hole center;¹³ ($\equiv\text{Si}-\text{O}-\text{O}\cdot$), consisting of an O_2^- radical ion bonded to a single silicon atom bonded to three oxygen atoms in the SiO_2 structure.^{24,25,30,31} The "small peroxy radical" is an alternative configuration, predicted by Edwards and Fowler,³² where the radical ion is strongly bonded to two silicon atoms, however it has not been observed in the common SiO_2 polymorph structures to date.²⁵ The NBOHC ($\equiv\text{Si}-\text{O}\cdot$) is described as a hole trapped in a pure $2p\pi$ orbital of a single oxygen bonded to a single silicon bonded to three oxygen atoms in the SiO_2 structure.^{13,25,33}

Evidence for nonparamagnetic defects in SiO_2 is obtained from absorption and luminescence spectroscopies, however ESR/EPR results strongly indicate the possible forms of nonparamagnetic precursors of the observed paramagnetic defects. The $B_{2\alpha}$ optical-absorption band at ~ 5.0 eV has been associated with the oxygen vacancy ($\equiv\text{Si}-\text{Si}\equiv$) from studies of oxygen-deficient SiO_2 (Ref. 34) and is a possible precursor of the E' center. The ~ 3.8 eV (Ref. 15) optical-absorption band has been associated with the peroxy linkages ($\equiv\text{Si}-\text{O}-\text{O}-\text{Si}\equiv$) from studies of oxygen-rich SiO_2 and from comparison with the SiO_2 local defect structure calculations of O'Reilly and Robertson.³³ Peroxy linkages are possible precursors of the peroxy radical and/or the NBOHC. However, peroxy radicals can also occur in oxygen-deficient SiO_2 (i.e., SiO_2 with a $B_{2\alpha}$ optical-absorption band indicating the presence of oxygen vacancies), and are believed to result from the reaction between an E' center and interstitial molecular oxygen^{15,18,32} (i.e., $\equiv\text{Si}\cdot + \text{O}_2 \rightarrow \equiv\text{Si}-\text{O}-\text{O}\cdot$). The 3.8 and 5.0 eV bands can be observed in a single spectrum implying that peroxy linkages and oxygen vacancies coexist in a single specimen,³⁵ depending on the method of synthesis of the SiO_2 .¹⁵ The peroxy linkage and the neutral oxygen vacancy are a Frenkel defect pair,^{11,13,24} but specimens with different peroxy linkage and oxygen vacancy concentrations will not be configured as such. The defect species induced by irradiation are strongly dependent on the existing precursors and therefore on the stoichiometry or absolute deficiency or excess of oxygen atoms over silicon atoms.^{15,34,36,37}

In natural and synthetic quartz, hydrogen and aluminum are the most common impurities.^{12,38} Hydrogen is incorporated as hydroxyl groups which tend to cluster in pairs¹³ (i.e., $\equiv\text{Si}-\text{OH HO}-\text{Si}\equiv$) in SiO_2 .^{11,30} Alternatively, atomic and molecular hydrogen are found interstitially. Atomic hydrogen which is mobile at 77 K,¹⁷ dimerizes at temperatures above 130 K,¹³ and the resultant molecular hydrogen becomes mobile in the range 170–230 K.²² Aluminum (Al^{3+}) substitutes for silicon in SiO_2 and is associated with alkali cations [mobile at temperatures above 200 K (Ref. 17)] which are local charge compensators. For high purity Sawyer premium Q -grade synthetic quartz,³⁹ which has an average aluminum concentration of 2 parts per million (ppm), the interstitial

charge compensators are H^+ , Li^+ , and Na^+ .

In Table I the results of some frequently cited luminescence experiments on SiO_2 polymorphs are summarized.^{1,9,13,23,28,40–60} The results of the present study are also included for comparison. In SiO_2 the dominant observed defects are in the short-range order⁴³ involving the SiO_2 tetrahedra fundamental to the SiO_2 structure.⁶¹ Silicate structure is determined by silicon-silicon and silicon-oxygen interactions rather than interactions between oxygen atoms.⁶¹ Thus, as shown in Table I, the defect structure and the resulting luminescence from amorphous and crystalline SiO_2 are similar.⁴³

II. EXPERIMENTAL DETAILS

Z-cut premium Q -grade synthetic high-purity quartz obtained from Sawyer Research Products Inc.³⁹ was investigated. The inclusion and dislocation densities, and impurity concentrations, are well characterized for this readily available commercial material. The maximum impurity concentrations were determined by Sawyer Research Products Inc.³⁹ for the particular specimens using the Q infrared quality factor method described by Brice.⁶² The impurities and their concentrations were determined to be OH (< 300 ppm), Al (< 2 ppm), Na (< 2 ppm), Li (< 2 ppm) with negligible amounts of common impurities such as Ge, K, Ca, and Fe. The particular quartz specimens studied were specifically manufactured for optical applications and therefore have a low inclusion density.

A number of complementary investigations of Sawyer premium Q -grade synthetic quartz have been reported in the literature and are available for comparison. They include CL,^{58,63} PL,^{44,52} thermoluminescence,^{21,23,64} optical-absorption spectroscopy,⁵² ESR,^{12,14,17,20,23,26,64} EPR,^{65,66} and infrared absorption spectroscopy.^{12,64,67} The optical-absorption spectroscopy of Sawyer Z-cut premium synthetic quartz⁵² reveals an absorption at 5.2 eV which is attributed to a transition involving an electron associated with an oxygen vacancy.^{34,52} The 3.8 eV optical absorption which has been observed in oxygen-rich SiO_2 (Refs. 15, 37, and 68) and has been associated with peroxy linkages was not detected from unirradiated premium synthetic quartz.⁵²

Therefore it is concluded that the Sawyer premium synthetic quartz is oxygen deficient (i.e., the preirradiation concentration of peroxy linkages is small, while the oxygen vacancy concentration is significant). This is an important distinction as the absolute and relative proportions of impurities and point defects have a profound effect on the irradiation sensitive defect structure and therefore on the identification of the CL from quartz. Z-cut specimens of the high-purity Sawyer premium synthetic quartz and for comparison, natural clear α -quartz from Oban NSW Australia, were polished to an optical finish. The specimens were coated with a thin conducting layer of carbon prior to irradiation to prevent deflection of the incident electron beam by charging of the specimen surface. The thickness of the carbon film was determined to be 30 ± 4 nm using a Park Scientific Autoprobe LS atomic force microscope. The specimens were not ir-

TABLE I. A comparison of the results of some frequently cited luminescence experiments on SiO₂ polymorphs.

Reference	SiO ₂	Excitation	Emission	Identification
28(1976)	<i>a</i> -SiO ₂ <i>α</i> -SiO ₂	CL	1.9 eV 2.5 eV 2.9 eV 4.28 eV 4.77 eV	<i>a</i> -SiO ₂ associated with <i>E'</i> center <i>α</i> -SiO ₂ associated with <i>E'</i> center
40(1979)	Quartz	X ray/UV	2.6 eV	STE
41(1980)	SiO ₂ films	CL	1.91 eV 2.21 eV 2.99 eV	Associated with residual or adsorbed water Intrinsic electron-beam-induced effect Impurity (implanted carbon)
42(1980)	SiO ₂ films	CL	1.9 eV 2.7 eV	Associated with <i>E'</i> center
43(1981)	Silica	PL	1.9 eV	NBO defects (not necessarily trapped holes)
44(1983)	Pure <i>α</i> -SiO ₂ ^a	X ray	2.8 eV 2.9 eV 3.25 eV	Recombination of an electron with a hole trapped adjacent to an (Al-M ⁺) center
45(1984)	Silica	Pol ^b PL	2.65 eV	Triplet→singlet transition Si ₂ ⁰ intrinsic defect (CL↓asT↓)
46(1984)	High purity glass	X ray	4.3 eV 1.9 eV	Singlet→singlet transition Si ₂ ⁰ intrinsic defect NBOHC (neutral paramagnetic bond defect—NBO atom with a hole in the 2 <i>p</i> orbital)
47(1985)	Quartz	Pulsed CL	2.05 eV 2.58 eV 3.1 eV 3–1.75 eV	Fine structure (separation 0.122 eV) associated with molecular O ₂ ⁻ ion vibrations
13(1985)	SiO ₂ glasses	Review/PL	1.85 eV 1.95 eV 2.64 eV	NBOHC Drawing induced defect STE
48(1985)	Pure <i>α</i> -SiO ₂	ODMR ^c	2.6 eV 2.9 eV 3.1 eV	STE (oxygen vacancy/interstitial oxygen pair)
49(1985)	High purity glass	PL	2.0 eV 2.1 eV 2.65 eV	Intrinsic emission associated with high [OH] Intrinsic emission associated with low [OH]
50(1987)	Fused silica	PL	2.7 eV 3.1 eV	Intrinsic O ₂ ⁻ (molecular ion) emission band
51(1988)	Pure SiO ₂ glasses	<keV CL	1.95 eV 2.22 eV 2.75 eV	Increases as [OH] decreases Due to manufacturing process Intrinsic/metastable state
52(1988)	Pure <i>α</i> -SiO ₂ ^a	pol ^b PL	2.5 eV 2.8 eV	Extrinsic STE (<i>E'</i> center and negatively charged peroxy radical)
53(1989)	Silica glass	PL	2.7 eV	Triplet→ground-state transition of neutral oxygen vacancy defect (oxygen-deficient glass)
54(1989)	Fused Silica	PL	2.7 eV 3.1 eV	Si-related center Triplet→singlet emission of Ge with 2 bridging O atoms
55(1990)	<i>a</i> -SiO ₂ un/densified	Pulsed CL & PL	2.1 eV 2.8 eV	STE in <i>a</i> -SiO ₂ STE in <i>α</i> -SiO ₂
9(1990)	Natural quartz	CL	“Blue”	Observed when [Al] > 50 ppm
56(1990)	Silica glass	PL	1.9 eV	Radiative relaxation O(¹ D)→O(³ P)
57(1990)	High purity glass	PL	1.9 eV 2.0 eV	NBOHC (O-rich sample) peroxy linkage precursor NBOHC (OH-rich sample) nonbridging hydroxy precursor third type of NBOHC precursor?

Table I (Continued.)

Reference	SiO ₂	Excitation	Emission	Identification
58(1990)	Pure α -SiO ₂ ^a	CL	1.9 eV	Associated with oxygen vacancies STE in Ge-doped α -SiO ₂ at 295/80 K Intrinsic emission (not a composite) Impurity incorporated during growth Line features (0.09 eV separation) associated with O molecules
			2.4 eV/2.2 eV	
			2.6 eV	
			2.8 eV	
			3.2 eV	
23(1990)	Pure α -SiO ₂ ^a	TL	2.65 eV	Associated with (AlO ₄) ⁰ hole traps, preirradiation Al ³⁺ ions are charge compensated by alkali ions immobile at 80 K Associated with (H ₃ O ₄) ⁰ hole traps
			3.25 eV	
1(1992)	Natural quartz	Review/CL	1.9 eV	Dangling nonbridging oxygen ions
			2.2 eV	
			2.6 eV	
59(1992)	High purity glass	PL	1.9 eV	STE NBOHC (—OH or peroxy linkage precursors) In low-OH silicas; not STE Intrinsic emission associated with —O—O— defect Exhibits STE decay characteristics
			2.7 eV	
			3.1 eV	
			2–4 eV	
60(1994)	Natural quartz	TL	2.0 eV	Follows annealing: associated with Al—O—Al bonds Inversely proportional to Al concentration
			2.6 eV	
This work	Pure α -SiO ₂ ^a	CL	1.91 eV	NBOHC ^d or \equiv Si: NBOHC (—OH precursor) STE (from α -SiO ₂ outgrowths) Extrinsic emission STE associated with E'_2 center (stabilized by immobile H ⁰) STE (α -SiO ₂) associated with E'_1 center Intrinsic emission Associated with (Al-M ⁺) center
			1.95 eV	
			2.28 eV (295 K)	
			2.46 eV (295 K)	
			2.69 eV (80 K)	
			2.72 eV (80 K)	
			2.93 eV (295 K)	
3.12 eV (295 K)				

^aSawyer Research Products, Inc.

^bPolarized PL.

^cOptically detected magnetic resonance.

^dStrained Si—O bond and peroxy linkage precursors.

radiated or annealed prior to the CL investigations.

The CL experiments were performed in a JEOL JSM 35C SEM equipped with a cryogenic stage, and an Oxford Instruments MonoCL cathodoluminescence imaging and spectral analysis system. The CL was excited using a continuous stationary electron beam at normal incidence, and measured using a retractable parabolic mirror collector. Spectra over the wavelength range 350–850 nm were collected by photon counting using a Hamamatsu R2228 PMT with a 1200 line/mm grating, blazed at 500 nm. In energy space the CL emission bands generally have a Gaussian shape with asymmetric high- and low-energy exponential tails which are highly dependent on the type and concentration of impurities.³ Therefore CL spectra, collected as a function of wavelength λ (nm), were converted to energy E (eV). Note this conversion⁶⁹ also requires each CL emission intensity to be multiplied by λ^2 . The spectra were corrected for total instrument response which was determined using an Oriel calibrated standard lamps (tungsten and deuterium). The SiO₂ emissions are broad, with a full width at half maximum (FWHM) between 0.15–0.60 eV, therefore failure to correct for instrument response can lead to errors in the

band shapes and energy positions of the emissions. The majority of SiO₂ CL studies do not specify whether the spectra have been corrected for instrument response which may account for some of the discrepancies between published reports.

III. RESULTS

The CL spectra of ultrapure synthetic quartz and natural clear quartz are very similar.⁶³ The local intrinsic defects dominate the CL spectrum, and the major impurities such as aluminum are generally at a low level (\sim 20 ppm) in clear natural quartz.⁷⁰ In Fig. 1, 295 K CL spectra collected as a function of increasing irradiation time are presented. The CL emission was excited by continuous irradiation with a stationary electron beam of energy 30 keV and current 0.25 μ A at normal incidence. The electron beam was focused with an incident beam diameter of 0.6 μ m.³ Monte Carlo⁷¹ simulations indicate that the penetration depth of 30 keV electrons in quartz is \sim 8 μ m. The resolution of the experimental spectral data ranges between 0.03 eV at 2 eV and 0.07 eV at 3 eV. The experimental spectral data represented as scatter plots

were fitted with a multiparameter Gaussian function using a nonlinear least-squares curve fitting algorithm.⁷² The baseline offset and the position, width, and integrated area under the peak were iteratively refined to a tolerance of at least 0.05.⁷² The minimum number of Gaussian emissions necessary to achieve this level of refinement were used for fitting. The parameters were fitted independently for each spectrum. Input parameters for the fitting procedure include only the number of peaks and an initial approximate estimate of their positions, determined from inspection of the experimental data.

In Fig. 1, the *dashed line* plots are the calculated fitted Gaussian components which are summed to produce the calculated fitted *solid line* plots for direct comparison with the experimental *scatter* plots. In Fig. 2, the CL emission intensities of the resolved Gaussian components (a sample of which are shown in Fig. 1) are plotted as a function of irradiation time. In Fig. 3, the same experiments are repeated with a defocused beam of diameter 15

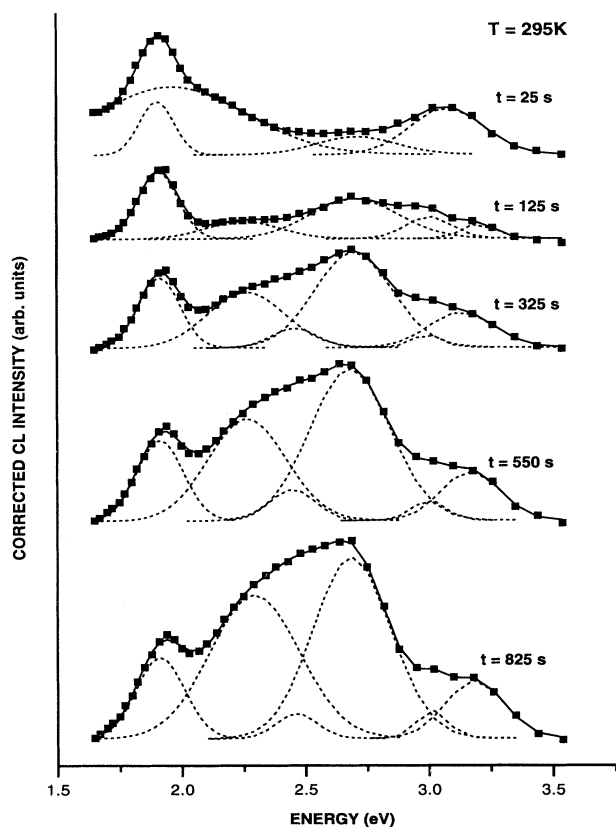


FIG. 1. A sample of the experimental CL spectra from quartz following normal stationary focused beam irradiation of energy 30 keV and current $0.25 \mu\text{A}$ at 295 K is represented by scatter plots. The estimated maximum uncertainty in the CL emission intensities is $\sim 5\%$ at ~ 3 eV where the system response is poor, and $< 0.5\%$ at ~ 2 eV where the system response is optimized. The dashed line plots are calculated fitted Gaussian components, which when summed result in the calculated fitted CL spectra represented as solid line plots.

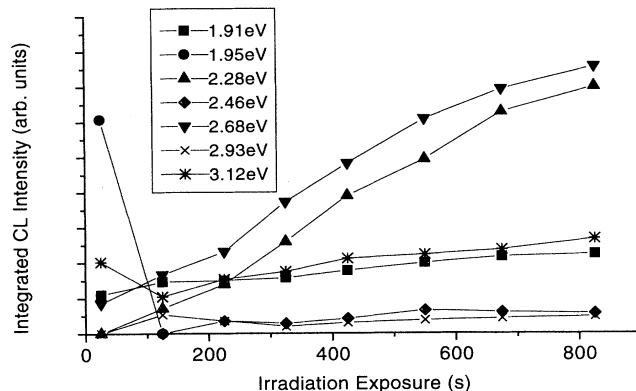


FIG. 2. The integrated CL intensities of the resolved calculated fitted Gaussian components of the CL spectra produced by focused beam irradiation at 295 K (see Fig. 1) are plotted as a function of irradiation exposure.

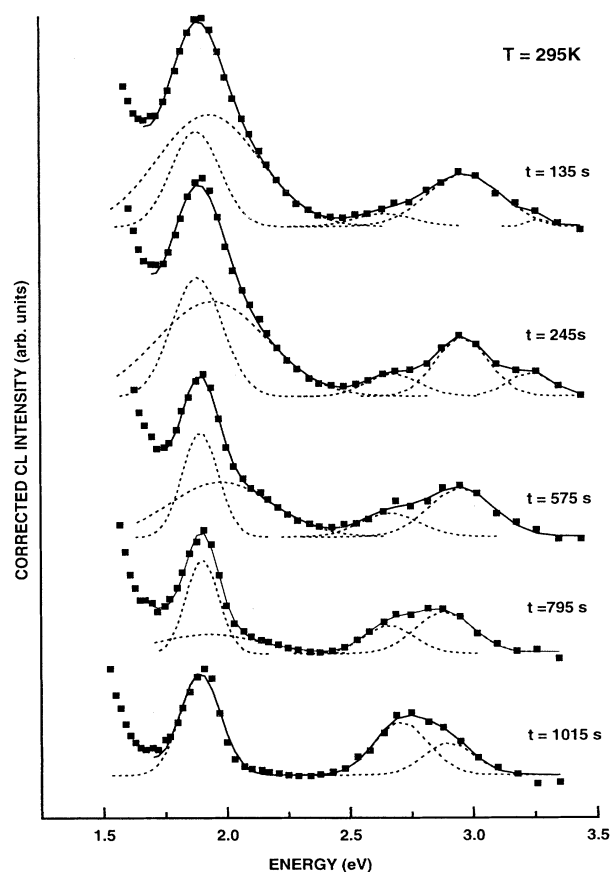


FIG. 3. A sample of the experimental CL spectra from quartz following normal stationary irradiation of increasing duration, with a defocused electron beam of energy 30 keV and current $0.25 \mu\text{A}$ at 295 K is presented by scatter plots. The dashed line plots are calculated fitted Gaussian components, which have been summed to produce the calculated fitted CL spectra, represented as solid line plots.

μm , energy of 30 keV, and current of $0.25 \mu\text{A}$. Thus the power density in the interaction volume has been reduced which results in the electron-beam-induced changes occurring at a slower rate. This enables in particular the growth and decay of the radiation sensitive 1.95 eV emission to be monitored. In Fig. 4, the CL emission intensities of the resolved Gaussian components in Fig. 3 are plotted as a function of irradiation time.

The experiment was repeated at 80 K using the identical focused beam parameters as used in Fig. 1, and is shown in Fig. 5. The ~ 2.7 eV emission increased by at least two orders of magnitude as the specimen was cooled from 295 to 80 K, in agreement with Luff and Townsend.⁵⁸ In Fig. 5, the ~ 2.7 eV feature in the $t = 725$ s spectrum has been fitted with both one and two Gaussian components for comparison. Visual inspection indicates that the two-component model better fits the experimental data (scatter plot). Where necessary statistical comparisons have been made to indicate which model provides a better fit. For this quantitative comparison commonly used numerical criteria of fit, generally known as reliability or R factors⁷³ have been adopted,

$$R_{\text{CL}} = \left\{ \frac{\sum [\text{CL}_i(\text{exp}) - \text{CL}_i(\text{fit})]^2}{\sum \text{CL}_i(\text{exp})^2} \right\}^{1/2},$$

where $\text{CL}_i(\text{exp})$ and $\text{CL}_i(\text{fit})$ represent the experimental and fitted CL intensities, respectively. The R factor provides merely a numerical comparison between models. It does not indicate whether a model is correct, unique, nor whether a better model exists. In Fig. 5, the R_{CL} factor for the single-component Gaussian model is 0.065 compared with an R_{CL} of 0.028 for the two-component Gaussian model. This confirms the visual assessment that the ~ 2.7 eV emission is more likely to be composed of at least two Gaussian components. Fitting three Gaussian components to the observed ~ 2.7 eV emission results in an R_{CL} of 0.025, which is not a significant improvement on the two-component fit and is therefore not justified by the quality of this set of data. In practice, a visually reasonable fit to the quartz spectra presented

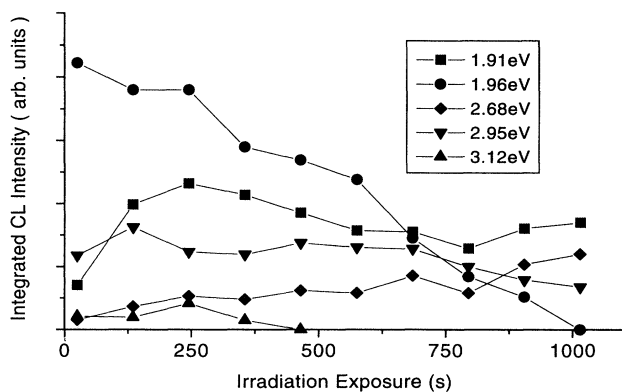


FIG. 4. The integrated CL intensities of the resolved calculated fitted Gaussian components of the CL spectra, produced by defocused beam irradiation at 295 K (see Fig. 3) are plotted as a function of irradiation exposure.

here corresponds to an R_{CL} of < 0.035 .

In Fig. 6, the CL emission intensities of the resolved Gaussian components in Fig. 5 are plotted as a function of irradiation time. In Table II, the mean CL emission position and mean FWHM of the resolved Gaussian bands shown in Figs. 2, 4, and 7 are summarized. The uncertainties indicate the maximum deviation from the mean peak position and mean FWHM determined at 295 and 80 K.

Comparison of Figs. 1 and 5 shows that the CL is strongly dependent on temperature as expected,³ however, beam-induced sample heating is frequently overestimated.⁷⁴ Filippov⁷⁵ has estimated the electron-beam-induced sample heating, by including a term to account for the penetration range of the incident electrons, rather than just the diameter of the incident beam, as in the commonly used estimations of Castaing,⁷⁶ Pittway, etc.³ Filippov's approach has been experimentally verified⁷⁷ using the temperature-sensitive sharp CL R line emission

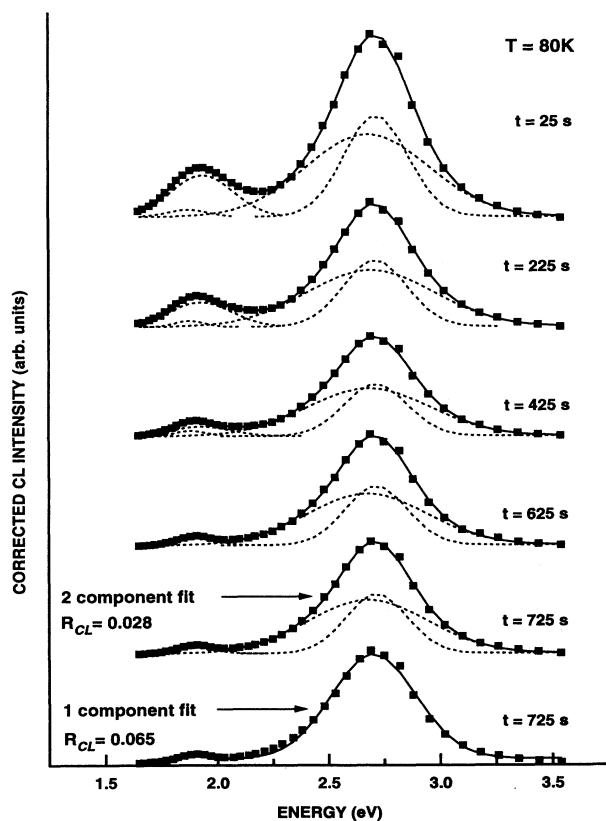


FIG. 5. A sample of the experimental CL spectra from quartz following normal stationary irradiation of increasing duration with a focused electron beam of energy 30 keV and current $0.25 \mu\text{A}$ at 80 K are represented by scatter plots. The dashed line plots are calculated fitted Gaussian components, which have been summed to produce the calculated fitted CL spectra, represented as solid line plots. The ~ 2.7 eV feature in the $t = 725$ s spectrum is fitted with both one and two Gaussian components for comparison. Visual and quantitative R_{CL} factor comparison indicates the broad feature at ~ 2.7 eV is likely to be composed of at least two Gaussian components.

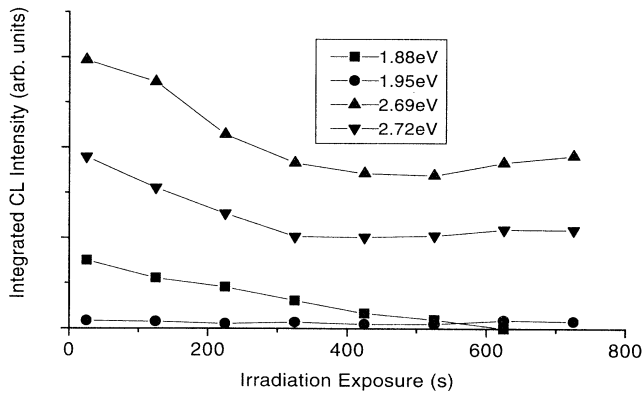


FIG. 6. The integrated CL intensities of the resolved calculated fitted Gaussian components of the CL spectra produced by focused beam irradiation at 80 K (see Fig. 5) are plotted as a function of irradiation exposure.

in $\text{Al}_2\text{O}_3:\text{Cr}^{3+}$. The increase in temperature induced by an electron beam with energy of 30 keV, current of 0.25 μA and beam diameter of 0.6 μm ,³ is therefore estimated⁷⁵ to be ~ 30 K at 295 K (heat capacity⁶² $C_{p_{295\text{K}}}$ is 0.74 $\text{J g}^{-1}\text{K}^{-1}$). At 80 K, the corresponding temperature-induced increase for the same beam parameters is < 10 K (heat capacity^{62,78} $C_{p_{80\text{K}}}$ is 0.25 $\text{J g}^{-1}\text{K}^{-1}$). Filippov has also devised an analytical expression estimating the time taken for the irradiation-induced temperature increase to stabilize.⁷⁵ These temperature changes are estimated to stabilize within milliseconds [where thermal conductivity $k_{295\text{K}}$ (Ref. 62) parallel to the c axis is 0.113 $\text{W cm}^{-1}\text{K}^{-1}$ and $k_{80\text{K}}$ (Refs. 62 and 78) is 0.5 $\text{W cm}^{-1}\text{K}^{-1}$] and therefore do not correlate with the observed changes in the CL spectra which occur over hundreds of seconds. Monitoring of the specimen block temperature with an Oxford Instruments platinum resistance sensor reveals no change (± 0.01 K) during irradiation at ambient temperature.

The importance of electron-beam-induced charging of insulators is well recognized.^{6-8,79} When carbon coated SiO_2 is irradiated with electrons, an electric field is induced due to the localization of charges at defects (either preexisting or radiolytically^{6,13} produced). Both natural and synthetic quartz charge rapidly during irradiation and this charge was maintained for long periods follow-

ing irradiation, as has previously been reported.^{6,7,63,80} No evidence of dielectric breakdown⁸⁰ was observed during any of the experiments.

IV. DISCUSSION

A sample of typical irradiation response spectra of the 1.9 eV CL emission is shown in the inset secondary plot in Fig. 7. The normalized 1.9 eV CL emission is plotted as a function of electron-beam irradiation time at 295 K. The specimen surface was continuously irradiated with a stationary electron beam of energy 30 keV and current 0.137 μA at normal incidence. Each spectrum was obtained from a previously unirradiated area of the specimen. While the electron-beam parameters were maintained for each spectrum, the power density delivered to each new interaction volume was varied by changing the area over which the specimen was irradiated, by defocusing the beam. From Fig. 7 it can be seen that the spectra are of similar form and the rate of development depends on the power density delivered to the interaction volume. The 1.9 eV CL irradiation response at 295 K is characterized by an initial rapid increase and maximizing of the luminescence, after which the emission decays until approximately stabilizing (slow decay) after longer irradiation times. These characteristic decay regions of each spectrum follow first-order kinetics in every case. Therefore the rate constants for the initial rapid and slow final decay regions were determined from the gradients of the $\ln(1.9\text{ eV CL intensity})$ versus irradiation time plots.

In Fig. 7, the rate constants for each of the decay regions are plotted as a function of power density in the interaction volume and initially the luminescence decay rate increases linearly as the power density increases. The final decay rate is constant and therefore independent of the power density, because the electron-beam irradiation-induced processes responsible for the 1.9 eV emission have achieved equilibrium within the interaction volume. Thus Fig. 7 shows that the 1.9 eV CL intensity varies in a characteristic manner during irradiation time, and confirms that the beam-induced reaction rates are correlated with the power density in the interaction volume, and hence the beam-induced electric field.

The sensitivity of the SiO_2 defect structure to irradiation is demonstrated and may account for some discrepancies reported in the literature (see Table I).

TABLE II. The mean CL emission positions and mean full width half maximum (FWHM) of the resolved Gaussian components (see Figs. 1, 3, and 5). The uncertainties indicate the maximum deviation from the mean emission positions and FWHM's determined at each temperature (295 and 80 K).

295 K		80 K	
Position (eV)	Width (eV)	Position (eV)	Width (eV)
1.91 \pm 0.01	0.20 \pm 0.04	1.88 \pm 0.02	0.17 \pm 0.02
1.95 \pm 0.05	0.42 \pm 0.06	1.95 \pm 0.02	0.32 \pm 0.04
2.28 \pm 0.03	0.39 \pm 0.05		
2.46 \pm 0.01	0.19 \pm 0.02		
		2.69 \pm 0.02	0.65 \pm 0.02
2.68 \pm 0.03	0.35 \pm 0.04	2.72 \pm 0.01	0.33 \pm 0.02
2.93 \pm 0.05	0.33 \pm 0.06		
3.12 \pm 0.05	0.37 \pm 0.04		

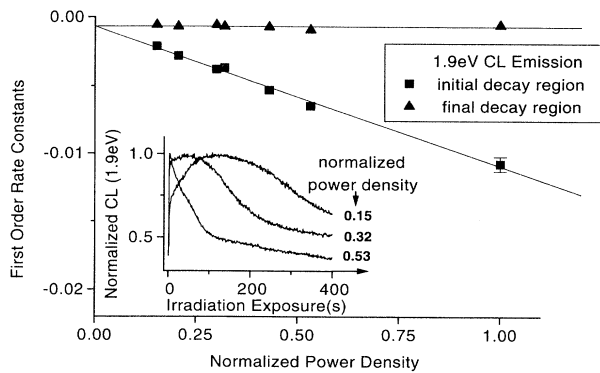


FIG. 7. The first-order rate constants of beam-induced processes involved in the ~ 1.9 eV CL emission are plotted as a function of the power density delivered by the incident beam. The rate constants are derived from CL irradiation response spectra including those in the inset secondary plot.

Therefore, although the processes are thermally assisted, it is concluded that the irradiation-induced electric field rather than irradiation-induced specimen heating is the major factor influencing the observed changes in the SiO_2 CL spectra resulting from irradiation at a particular temperature. The observed electron-beam-induced changes in the CL emission intensities are not correlated with the electron-beam-induced specimen heating, which stabilizes within milliseconds⁷⁵ for the described experiments. Electron-beam parameters were varied systematically, and it was found that for beam energies between 15 and 35 eV and beam currents between 0.1 and 0.3 μA , the CL emission response is of the same form with the reaction rates increasing as a function of power density. Hence the data presented in Figs. 1, 3, and 5 are representative of the typical response observed. It is noted that the irradiation response profile of the 1.9 eV emission is similar to that predicted by Cazaux and Le Gressus,⁷⁴ for the buildup and subsequent modification of trapped charge in an insulator due to specimen changes induced by electron irradiation.

A. 1.91 and 1.96 eV emissions

The widely reported SiO_2 emission at ~ 1.9 eV has been attributed to the recombination of electrons in the highly localized nonbridging oxygen band-gap state, with holes in the valance-band edge.³³ The NBOHC defect has been identified in SiO_2 by ESR/EPR,^{11,13,25,35,37,56,81} optical-absorption spectroscopy,^{18,19,35,37,49,57,82} luminescence spectroscopies (i.e., CL, PL, x-ray),^{1,13,41,43,46,49,56,59} and predicted by theoretical calculation.³³

A number of different precursors have been proposed for the NBOHC. The simultaneous existence of NBOHC arising from different precursors in a single specimen has been reported.^{13,35,49,57,59} In SiO_2 with appreciable hydroxyl concentration (i.e., $-\text{OH} > 200$ ppm), the radiolysis^{11,13} of the hydroxyl group leads to the formation of a NBOHC (Ref. 59) and the production of atomic hydrogen^{22,57} (i.e., $\equiv\text{Si}-\text{O}-\text{H} \rightarrow \equiv\text{Si}-\text{O}\cdot + \text{H}^0$).¹³

NBOHC's are also observed in SiO_2 with low hydroxyl

concentration³⁷ and therefore must evolve from precursors not involved with hydroxyl groups.⁴⁹ Nonbridging oxygen atoms, locally charge compensated by alkali cations, can also serve as precursor defects for the irradiation-induced NBOHC,⁴⁴ but the concentration of this type of precursor would be expected to be minimal in ultrapure synthetic SiO_2 . The optical-absorption spectrum enables SiO_2 with low hydroxyl concentration to be further classified as either oxygen-rich/surplus or oxygen deficient.⁶⁸ Oxygen-rich specimens typically have peroxy linkages⁵⁶ as indicated by the ~ 3.8 eV optical absorption,¹⁵ while oxygen-deficient specimens typically have oxygen vacancies^{34,53} as indicated by the $B_{2\alpha}$ optical-absorption band at ~ 5.0 eV.

In oxygen-rich specimens the peroxy linkages⁵⁶ provide likely precursors for NBOHC's^{57,59} and a number of different irradiation-induced transformations have been proposed (for example, $\equiv\text{Si}-\text{O}-\text{O}-\text{Si}\equiv \rightarrow \equiv\text{Si}-\text{O}\cdot-\text{O}-\text{Si}\equiv$).^{15,37} Apart from the hydroxyl and peroxy linkage precursors, a third precursor type is indicated by experiment:³⁷ The "strained" silicon-oxygen, ($\text{Si}-\text{O}$) bond^{6,13} which may exist due to excitation by irradiation is a possible NBOHC precursor ($\equiv\text{Si}-\text{O}-\text{Si}\equiv \rightarrow \equiv\text{Si}-\text{O}\cdot-\text{Si}\equiv$) and may also result in the formation of an E' center. These defects have also been detected during production of SiO_2 fibers in which context they are described as "drawing induced" defects.¹⁸

Optical-absorption spectroscopy⁵² and compositional analysis^{17,39} indicate that *unirradiated* Sawyer premium synthetic SiO_2 is oxygen deficient⁵² and has an $-\text{OH}$ concentration of < 300 ppm.³⁹ An alternative intrinsic defect^{13,49} proposed to account for the ~ 2 eV optical absorption in low OH materials is the "electron trap" or Si_3^- defect,¹³ which is three-coordinated silicon with a trapped electron (i.e., $\equiv\text{Si}\cdot$). The oxygen vacancy which is a defect commonly detected⁵² in Sawyer premium synthetic SiO_2 is a possible precursor for this (diamagnetic) trapped electron center (i.e., $\equiv\text{Si}-\text{Si}\equiv \rightarrow \equiv\text{Si}\cdot : \text{Si}\equiv + \text{H}^+$).¹³ The energy level associated with the Si_3^- defect⁴⁹ is predicted to be ~ 2 eV below the conduction band.³³

Optical absorptions^{35,57} associated with the NBOHC's with different precursors have been identified. A broad (~ 1 eV) absorption is observed at 2.1 eV from SiO_2 with 800 ppm $-\text{OH}$ concentration.⁵⁷ The simultaneous existence of two kinds of NBOHC's may account for the broadness, as a narrower absorption (~ 0.5 eV width) is observed at 1.975 eV from SiO_2 with a low OH concentration.³⁵ A small Stokes shift of 0.05 eV is theoretically predicted for the NBOHC.³³ The present investigation is consistent with the association of the NBOHC with $-\text{OH}$ precursor, with the CL emission observed at 1.95 eV. The irradiation of the hydroxy group at temperatures < 100 K,¹³ leads to the production of reactive atomic hydrogen H^0 which thermally diffuses when temperatures exceed 130 K and tends to dimerize. At temperatures above 170–200 K,¹³ the thermal migration of the resultant H_2 becomes significant. At temperatures exceeding 230 K,²² some of the NBOHC's and the H_2 molecules may recombine to reform a nonbridging hy-

droxy group ($\equiv\text{Si}-\text{OH}$),¹³ however the radiation response spectrum for this emission (Fig. 4) suggests that alternative diffusion limited¹³ processes operate: It is observed that the hydroxy group concentration within the interaction volume is strongly reduced by irradiation, resulting in the rapid attenuation of the associated CL emission at 1.95 eV.

The CL emission observed at 1.91 eV in Fig. 1 increases initially and stabilizes. Sawyer premium synthetic SiO_2 has a low concentration of preirradiation peroxy linkages; therefore the strained $\text{Si}-\text{O}$ bond^{13,57} is a more likely precursor for the NBOHC associated with this emission. The relative peak positions of the 1.91 and 1.95 eV emissions are consistent with optical-absorption measurements of the corresponding non-OH and -OH precursor NBOHC defects, at 1.975 and 2.10 eV, respectively,⁵⁷ considering the predicted³³ Stokes shift of 0.05 eV. Alternatively or additionally, the 1.91 eV emission may be associated with the Si_3^- defect.^{13,49} The Si_3^- defect precursor is the oxygen vacancy which is a common defect in Sawyer premium synthetic quartz.

It is noted that continuous stationary irradiation with a well focused electron beam for an extended period produces peroxy linkages.⁶³ It is proposed that a component of CL emission at ~ 1.9 eV, observed from irradiated Sawyer premium synthetic quartz is associated with the NBOHC with peroxy linkage precursor (see Sec. IV B).

B. 2.28 and 2.68 eV emissions

Tanimura, Tanaka, and Itoh⁸³ reported an electron-beam-induced volume change in α -quartz and fused silica. Irradiation produces excitons which are localized by a self-induced lattice distortion resulting in the observed volume increase.^{83,84} The lifetime of the self-trapped exciton (STE) is of order ~ 1 ms (Ref. 52) and hence the associated volume change is transient.^{83,85} The restoration of the original structure is associated with the radiative recombination of the STE.⁸⁴ In crystalline SiO_2 , this luminescence is observed between 2.6 and 2.8 eV,^{1,23,39,40,44,52,58} while pulsed electron irradiation of amorphous SiO_2 results in a luminescent emission between 2.2 (Ref. 55) and 2.4 eV.⁸⁵ Experimental^{1,13,48,52,83-86} and theoretical^{27,87-89} investigations of the STE in SiO_2 have led to the proposal of a number of different models. Hayes *et al.*⁴⁸ proposed that the STE involves an irradiation-induced transient oxygen Frenkel pair comprised of an oxygen vacancy and a peroxy linkage.⁶ ESR experiments have shown that E' center variants are produced in abundance by a radiolytic process.¹³ Therefore it has been proposed that the radiolysis⁶ of the $\text{Si}-\text{O}$ bond results in either a transient localized E' center and peroxy linkage pair,^{37,83} an E' center and negatively charged peroxy radical pair,⁵² or an E' center and NBOHC pair.¹³ In Fig. 1 the emission at 2.68 eV is assigned to the radiative recombination of the STE produced by the radiolysis of $\text{Si}-\text{O}$ bonds in the interaction volume. The 2.68 eV emission is observed to increase in intensity with irradiation exposure. This is due to the migration of competing radiative and nonradiative centers out of the interaction volume under the influence of the

beam-induced electric field.

Electron irradiation of an insulator at normal incidence produces a symmetric charge distribution which induces an electric field. Cazaux^{7,79} has characterized this electric field in terms of radial (parallel to the surface) and axial (normal to the surface) components. The preexisting and irradiation-induced negatively charged species such as oxygen defect centers migrate towards the surface,⁷⁹ under the influence of the axial electric field. The radial field is null along the z axis and at the quartz/carbon interface, and is only significant at μm depths below the coated surface.⁷⁹ In a SEM, the spatial distribution of defects identified with particular CL emissions may be mapped using monochromatic CL imaging. Figure 8 shows a panchromatic (all wavelengths between 300–900 nm) CL micrograph of a specimen previously irradiated with a continuous stationary electron beam of energy 30 keV and current of $0.25 \mu\text{A}$ at normal incidence. The localized circular CL images⁶³ result from a series of irradiations of 15, 20, 45, 60, 75, 90, 105, and 200 s duration. This series of CL images in Fig. 8 is representative of the reproducible irradiation-induced evolution of the images. Initially the irradiated region uniformly luminesces, however as irradiation continues the luminescent intensity is enhanced first at the boundary and then, following further irradiation, in the central region.

The change in the CL image is directly correlated with the electromigration of oxygen defect centers which result in the oxygen enrichment of the irradiated surface region, consistent with electron probe microanalysis (EPMA) observations.⁸ The accumulated oxygen is incorporated into the quartz surface structure as peroxy linkages, the formation of which results in a permanent volume increase observed as amorphous SiO_2 on crystal-

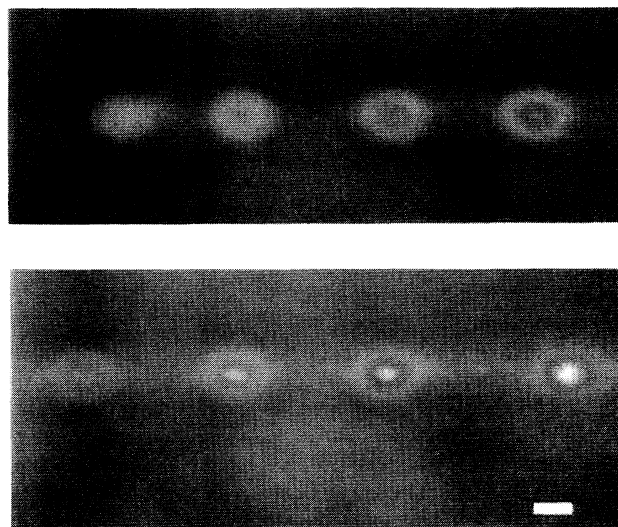


FIG. 8. Panchromatic CL micrograph of quartz previously irradiated with a normal focused stationary electron beam at 295 K for (top row, left to right) 15, 30, 45, 60 s and (second row, left to right) 75, 90, 105, and 200 s duration. The dimension marker is representative of $10 \mu\text{m}$.

line SiO₂.⁶³ Monochromatic CL imaging of the 2.28 eV emission reveals it is restricted to and correlated with the development of the outgrowth. Note that in amorphous SiO₂, the STE emission is observed between 2.2 (Ref. 55) and 2.4 eV (Ref. 85) consistent with this proposed identification.⁶³ The irradiation response and the peak widths of the 2.28 eV emission and the 2.69 eV emission in Fig. 2 are very similar. Therefore the 2.28 eV emission is assigned to the relaxation of the irradiation-induced STE within the outgrowth.

It is noted that ~ 1.9 eV emission is also observed from the central outgrowth region, where the 2.28 eV emission is localized. The FWHM of the 1.91 eV CL emission linearly ($\pm 7\%$) increases from 0.16 to 0.23 eV during 825 s irradiation by the focused electron beam. It is likely that the observed increase is due to the growth of a new unresolved emission. The width of the 1.91 eV emission does not increase *unless* emission is observed from the central outgrowth region. The concentration of the irradiation produced peroxy linkage defects⁶³ is significant only in the outgrowth. Therefore it is proposed that this emission from the oxygen-rich outgrowth is associated with the NBOHC with peroxy linkage precursor.

At 80 K, the thermal assistance of the migration of defects is reduced, and the role of hydrogen in the defect structure of SiO₂ is particularly important. In Fig. 5, the ~ 2.7 eV emission at 80 K may be resolved into at least two components, as described previously. The component with FWHM of ~ 0.35 eV is observed between 295 and 80 K and is assigned to the radiative recombination of the STE associated with an E'_1 . In α -quartz the four tetrahedrally configured oxygen atoms surrounding the silicon are pairwise equivalent,¹² and usually described as having either "short" (1.598 Å) or "long" (1.616 Å) bonds.¹² Thus two inequivalent relaxations resulting in the formation of an E' center are possible at the site of an oxygen vacancy.¹⁶ ESR experiments¹⁶ have associated the energetically more favorable E'_1 center with the short bond, while the E'_2 center is associated with the long bond and is usually¹⁶ but not always²⁷ stabilized by a proton.¹⁶ The radiolysis of the nonbridging hydroxy group at 80 K results in the production of a NBOHC and atomic hydrogen. At 295 K, the resultant thermally mobile hydrogen dimerizes and rapidly diffuses. At 80 K, the atomic hydrogen is much less mobile and is therefore available to stabilize the energetically less favorable E'_2 center.¹⁶ The E'_2 center becomes thermally unstable at temperatures exceeding 170 K^{13,32} when dimerization and diffusion of hydrogen become significant processes.

It is possible that the broad emission at 80 K may also have contributions associated with the STE from the amorphous outgrowth. However the spectral resolution is not sufficient to enable these components to be identified. As described previously, the only impurities in Sawyer premium synthetic quartz¹³ present in significant concentrations are Al³⁺, Na⁺, Li⁺, and H⁺. However the concentration of Na⁺, Li⁺, and H⁺ and other positively charged interstitial defect centers in the amorphous outgrowth is expected to be negligible, because of electromigration due to the irradiation-induced electric field.

In Sawyer premium synthetic quartz¹³ the Al³⁺ impurities substitute for Si⁴⁺ and are less likely to migrate than the interstitial species.

The large increase in the emission associated with the STE from the interaction volume occurs because competitive thermally assisted (diffusion limited) radiative and nonradiative processes occurring within the interaction volume are reduced or inactive at 80 K. The volume of the amorphous outgrowth is estimated to be of order 2.5% of the crystalline interaction volume and therefore the contribution of the radiative recombination of the STE from the amorphous outgrowth is likely to be correspondingly small. At 295 K, the STE emission from the amorphous outgrowth is comparable with the STE emission from the interaction volume. This is because competitive processes due to positively charged defect centers (i.e., Na⁺, Li⁺, and H⁺) are negligible within the amorphous outgrowth at both 295 and 80 K. This is in contrast to the situation in the interaction volume at 295 K where the positively charged defect center concentration and associated competitive thermally assisted processes are significant. Thus the emission from the recombination of the STE from the crystalline interaction volume is reduced with respect to the corresponding emission from the recombination of the STE from the amorphous outgrowth at 295 K.

Additionally at 80 K, it is likely that the extremely reactive atomic hydrogen produced by the radiolysis of the hydroxy groups bond with the E' centers, which are produced in abundance at 80 K, will react such that ($\equiv \text{Si} \cdot + \text{H}^0 \rightarrow \equiv \text{Si}-\text{H}$).¹³ The operation of this process would account for the observations of the irradiation response of the CL emission shown in Fig. 7: The ~ 2.7 eV emission associated with the STE decreases in intensity as the 1.95 eV emission associated with the —OH precursor NBOHC decreases. Atomic hydrogen is produced during the attenuation of the 1.95 eV emission and a proportion of this hydrogen will bond with the E' centers. The bonding of the E' centers and atomic hydrogen results in a nonbridging hydrogen configuration and therefore competes with the metastable STE configuration. Thus emission associated with the relaxation of the STE is reduced. Further it is noted that following the decay of the emission at 1.95 eV associated with the —OH precursor NBOHC, the emission associated with the STE stabilizes. This is because the available hydroxy groups have been dissociated within the interaction volume and the source of atomic hydrogen is no longer available to enable the suggested competing process to operate.

C. 2.46 eV emission

Itoh, Tanimura, and Itoh⁵² observed a PL emission from Sawyer premium synthetic quartz at 2.5 eV, and assigned it to an extrinsic process. This emission is not immediately obvious from visual inspection of the experimental spectra in Fig. 1, due to the close proximity of more intense emissions. Input parameters for the fitting procedure include the number of peaks and their approximate position which are usually determined from inspection of the experimental data. The experimental CL

spectra in Fig. 1 for irradiation times exceeding 250 s were fitted with and without an emission at ~ 2.5 eV. It was found that when the ~ 2.5 eV emission was included, slightly better fits were obtained with the experimental data, indicated both visually and by an improvement of R_{CL} . Furthermore, unless an emission at ~ 2.5 eV is included, a discontinuity in the calculated irradiation response of the integrated CL intensity of the 2.28 eV emission is observed, after ~ 250 s irradiation with beam parameters as described. When the spectra are fitted without the ~ 2.5 eV emission, the rapid increase in the calculated integrated intensity is mainly due to an $\sim 25\%$ increase in the FWHM of the calculated Gaussian 2.28 eV component. When the spectra are fitted with the ~ 2.5 eV emission, no discontinuities or rapid changes in the FWHM are observed in the calculated irradiation response of the 2.28 eV emission. Therefore the refined emission energy was determined to be 2.46 ± 0.01 eV and as can be seen in Fig. 2, the CL emission at 2.46 eV saturates following irradiation, in agreement with the observations of the 2.5 eV PL emission.⁵² Thus the present study indicates the existence of an emission at 2.46 eV and is consistent with the observations of Itoh, Tanimura, and Itoh,⁵² although the resolution of the CL spectroscopic data is not sufficient to warrant an independent visual identification.

D. 3.12 eV emission

A luminescent emission observed^{12,23,44} between 3.1–3.25 eV has been attributed to the recombination of a hole trapped adjacent to a substitutional, charge-compensated aluminum-alkali ion center ($Al-M^+$).^{12,23,44} The Al^{3+} substitutes for Si^{4+} , thus requiring charge compensators which in ultrapure Sawyer premium synthetic quartz³⁹ are localized interstitial H^+ , Li^+ , and Na^+ . In addition following irradiation, a hole trapped in a non-bonding oxygen p orbital may also be associated with the substitutional Al^{3+} .^{12,23} Irradiation of SiO_2 is known to result in the release of atomic hydrogen at temperatures above 77 K (Ref. 12) and alkali metals at temperatures above 200 K,²⁶ followed by their diffusion which is facilitated along the c axis channels in α -quartz.^{17,32}

Thus the initial rapid attenuation of the 3.12 ± 0.05 eV emission in Fig. 1 associated with the ($Al-M^+$) center results from the dissociation and thermally assisted electromigration of the charge compensators out of the interaction volume under the influence of the irradiation-induced electrical field.^{7,79} This interpretation is consistent with x-ray photoelectron spectroscopy⁹⁰ depth-profile studies which show that sodium is depleted from the interaction volume by electron irradiation. Sodium concentration in excess of the bulk concentration is found at the periphery of the interaction volume, providing strong evidence for electromigration. Following the initial rapid attenuation, the 3.12 eV emission intensity stabilizes and then steadily increases as irradiation continues (Fig. 2). The increase in emission is strongly correlated with the loss of the conductive carbon coating,^{63,79} which results in alternation⁷⁹ of the irradiation-induced electric field within the specimen, causing the electromigration of

alkali cations back into the interaction volume. The subsequent reassociation of the ($Al-M^+$) center accounts for the increase in the 3.12 eV emission. This interpretation is consistent with EPMA studies⁷⁹ of SiO_2 glass where following an initial decrease, the Na^+ signal was observed to increase when the conductive coating was destroyed.

The aluminum concentration (average concentration < 3 ppm) was found to be nonuniform in Sawyer premium synthetic quartz. This was indicated by the varying intensity of the 3.12 eV emission associated with the ($Al-M^+$) center as different regions of the specimens were irradiated. This is consistent with the observations of Luff and Townsend⁵⁸ of an emission at 3.2 eV from Sawyer premium synthetic quartz. They noted the CL emission (attributed to defects incorporated during growth⁵⁸) varied in intensity from different areas of the specimen. The possibility that the broad 2.69 eV emission observed at 80 K in Fig. 5 may have contributions from the ($Al-M^+$) center is not discounted. Improved stability of the ($Al-M^+$) center is to be expected due to the immobility of the alkali cations (Li^+) and (Na^+) at temperatures < 200 K.¹⁷ The spectral resolution of the experimental data is not sufficient to enable this distinction.

TABLE III. The emission bands observed in the 295 and 80 K CL spectra of ultrapure synthetic quartz are identified.

Position (eV) (FWHM)		Identification
295 K	80 K	
1.91 (0.20)	1.88 (0.17)	Associated with NBOHC with Si—O, and post irradiation peroxy linkage precursors or $\equiv Si:$ center
1.95 (0.42)	1.95 (0.32)	Associated with NBOHC with —OH precursor
2.28 (0.39)		Radiative recombination of a STE from α - SiO_2 outgrowth
2.46 (0.19)		Extrinsic emission?
	2.69 (0.65)	Radiative recombination of a STE from α - SiO_2 , associated with an E'_2 center stabilized by immobile H^0
2.68 (0.35)	2.72 (0.33)	Radiative recombination of a STE from α - SiO_2 , associated with an E'_1 center and either a peroxy radical, peroxy linkage, or NBOHC
2.93 (0.33)		Intrinsic emission?
3.12 (0.37)		Associated with the charge compensated, substitutional [$Al-M^+$] center where M^+ is Li^+ , Na^+ , or H^+

E. 2.93 eV emission

The spectra in Fig. 3 were obtained irradiating an area of relatively low aluminum concentration, as indicated by the relatively low 3.12 eV emission intensity (in contrast with the spectra in Fig. 1). This enabled an emission at 2.93 ± 0.28 eV to be resolved. The observed irradiation response is similar to the intrinsic 1.91 eV emission rather than the 3.12 eV emission associated with the aluminum impurity or the 1.95 eV emission associated with —OH precursors. Thus the 2.93 eV emission is possibly associated with an irradiation produced intrinsic defect. An emission between 2.9–3.1 eV has been previously reported.^{28,41,44,47,50,59} Alonso *et al.*⁴⁴ determined that in Sawyer premium synthetic quartz the emission is not correlated with the (Al- M^+) center consistent with the results in Fig. 2. The ~ 2.95 eV emission has also been variously associated with a carbon impurity,⁴¹ an —O—O— type defect⁵⁹ or O_2^- defects.^{47,69}

V. CONCLUSIONS

The emission bands observed in the 295 and 80 K CL spectra of ultrapure Sawyer premium Q -grade synthetic quartz have been associated with various defect centers. These identifications are listed in Table III and may be compared with the results of other luminescence experiments on SiO_2 polymorphs, summarized in Table I. The experimental CL spectra, corrected for total instrument response, were fitted using a nonlinear least-squares multiparameter Gaussian function. A numerical criterion (R_{CL} factor) was adopted to assist with the assessment of the quality of the fit. This work has characterized previously unreported CL emissions from α - SiO_2 which have been associated with defect centers consistent with those determined using complementary methods such as ESR, EPR, optical-absorption spectroscopy, and PL, etc. The

assignment of the observed CL emission to particular defect centers will allow the defect center concentration and distribution to be monitored. CL microscopy (imaging) enables the individual emissions associated with particular defect centers to be mapped with high sensitivity and spatial resolution. Thus CL microscopy and spectroscopy are ideal techniques for the microcharacterization of the defect structure of SiO_2 and other technologically important luminescent materials.

Previous work indicates that the defect structure and defect formation mechanisms are dependent on the method of manufacture. The preirradiation concentration of hydroxy groups,^{19,30,35,59} oxygen vacancies (i.e., oxygen-deficient specimen),^{49,52,53,57,59,82} peroxy linkages (i.e., oxygen surplus specimen),^{13,15,37,57} and the concentration and spatial distribution of the common impurities (H, Al, Na, Li, Ge, C, etc.) are determined by the method of manufacture. This work has demonstrated the sensitivity of the SiO_2 defect structure to specimen temperature and electron irradiation. The irradiation-induced electromigration of defect species has important consequences for the interpretation and application (i.e., choice of beam parameters) of electron probe techniques. In addition irradiation enables the micromanipulation of the spatial distribution and type of defect, impurity and/or dopant. This useful property may have applications in "nanotechnology" and the development of nanofabrication techniques.

ACKNOWLEDGMENTS

Helpful discussions with A. R. Moon, the assistance of A. R. Giles in the preparation of the quartz samples, and the technical support provided by R. Wuhler are gratefully acknowledged. M.A.S.K. acknowledges financial support from Insearch Ltd.

- ¹G. Remond, F. Cesbron, R. Chapoulie, D. Ohnenstetter, C. Rouques-Carmes, and M. Schvoerer, *Scanning Microsc.* **6**, 23 (1992).
- ²J. W. Steeds, in *Encyclopedia of Applied Physics*, edited by G. L. Trigg (VCH Publishers, New York, 1992), Vol. 3, p. 121.
- ³B. G. Yacobi and D. B. Holt, *Cathodoluminescence Microscopy of Inorganic Solids* (Plenum, New York, 1990).
- ⁴B. G. Yacobi and D. B. Holt, *J. Appl. Phys.* **59**, R1 (1986).
- ⁵D. B. Holt, *Scanning Microsc.* **6**, 1 (1992).
- ⁶J. P. Vigouroux, J. P. Durad, A. Le Moel, C. Le Gressus, and D. L. Griscom, *J. Appl. Phys.* **57**, 5139 (1985).
- ⁷J. Cazaux, *J. Microsc. Spectrosc. Electron.* **11**, 293 (1986).
- ⁸M. Fialin and G. Remond, *Microbeam Anal.* **2**, 179 (1990).
- ⁹K. Ramseyer and J. Mullis, *Am. Miner.* **75**, 791 (1990).
- ¹⁰U. Zinkernagel, *Contrib. Sedimentology* **8**, 1 (1978).
- ¹¹D. L. Griscom and E. Friebele, *Phys. Rev. B* **34**, 7524 (1986).
- ¹²L. E. Halliburton, N. Koumvakalis, M. E. Marques, and J. J. Martin, *J. Appl. Phys.* **52**, 3565 (1981).
- ¹³D. L. Griscom, *J. Non-Cryst. Solids* **73**, 51 (1985).
- ¹⁴D. L. Griscom, *Phys. Rev. B* **40**, 4224 (1989).
- ¹⁵N. Nishikawa, R. Tohmon, Y. Ohki, K. Nagasawa, and Y. Hama, *J. Appl. Phys.* **65**, 4672 (1989).

- ¹⁶D. L. Griscom, *Phys. Rev. B* **22**, 4192 (1980).
- ¹⁷M. E. Marques and L. E. Halliburton, *J. Appl. Phys.* **50**, 8172 (1979).
- ¹⁸H. Hanafusa, Y. Hibino, and F. Yamamoto, *J. Non-Cryst. Solids* **95**, 655 (1987).
- ¹⁹E. J. Friebele and M. E. Gingerich, *J. Non-Cryst. Solids* **38&39**, 245 (1980).
- ²⁰R. B. Bossoli, M. G. Jani, and L. E. Halliburton, *Solid State Commun.* **44**, 213 (1982).
- ²¹R. Chen, X. H. Yang, and S. W. S. McKeever, *J. Phys. D* **21**, 1452 (1988).
- ²²D. L. Griscom, M. Stapelbroek, and E. J. Friebele, *J. Chem. Phys.* **78**, 1638 (1983).
- ²³X. H. Yang and S. W. S. McKeever, *J. Phys. D* **23**, 237 (1990).
- ²⁴E. J. Friebele, D. L. Griscom, M. Stapelbroek, and R. A. Weeks, *Phys. Rev. Lett.* **42**(20), 1346 (1979).
- ²⁵D. L. Griscom and E. J. Friebele, *Phys. Rev. B* **24**, 4896 (1981).
- ²⁶M. G. Jani, R. B. Bossoli, and L. E. Halliburton, *Phys. Rev. B* **27**, 2285 (1983).
- ²⁷F. J. Feigl, W. B. Fowler, and K. L. Yip, *Solid State Commun.* **14**, 225 (1974).

- ²⁸C. E. Jones and D. Embree, *J. Appl. Phys.* **47**, 5365 (1976).
- ²⁹J. F. Conley, P. M. Lenahan, H. L. Evans, R. K. Lowery, and T. J. Morthorst, *Appl. Phys. Lett.* **65**, 2281 (1994).
- ³⁰M. Stapelbroek, D. L. Griscom, E. J. Friebele, and G. H. Sigel, *J. Non-Cryst. Solids* **32**, 313 (1979).
- ³¹J. M. Baker and P. T. Robinson, *Solid State Commun.* **48**, 551 (1983).
- ³²A. H. Edwards and W. B. Fowler, *Phys. Rev. B* **26**, 6649 (1982).
- ³³E. P. O'Reilly and J. Robertson, *Phys. Rev. B* **27**, 3780 (1983).
- ³⁴R. Tohman, Y. Mizuno, K. Ohki, K. Sasagane, K. Nagasawa, and Y. Hama, *Phys. Rev. B* **39**, 1337 (1989).
- ³⁵K. Nagasawa, Y. Hoshi, and Y. Ohki, *Jpn. J. Appl. Phys.* **26**, L554 (1987).
- ³⁶K. Nagasawa, Y. Hoshi, Y. Ohki, and K. Yahagi, *Jpn. J. Appl. Phys.* **25**, 464 (1986).
- ³⁷H. Nishikawa, R. Karamura, R. Tohmon, Y. Ohki, Y. Sakurai, K. Nagasawa, and Y. Hama, *Phys. Rev. B* **41**, 7828 (1990).
- ³⁸J. C. Brice, *Rev. Mod. Phys.* **57**, 105 (1985).
- ³⁹Sawyer Research Products Inc., Eastlake, Ohio 44095.
- ⁴⁰A. N. Trukhin and A. E. Plaudis, *Sov. Phys. Solid State* **21**, 644 (1979).
- ⁴¹H. Koyama, *J. Appl. Phys.* **51**, 2228 (1980).
- ⁴²S. W. McKnight and E. D. Palik, *J. Non-Cryst. Solids* **40**, 595 (1980).
- ⁴³G. H. Sigel and M. J. Marrone, *J. Non-Cryst. Solids* **45**, 235 (1981).
- ⁴⁴P. J. Alonso, L. E. Halliburton, E. E. Kohnke, and R. B. Bosoli, *J. Appl. Phys.* **54**(9), 5369 (1983).
- ⁴⁵L. N. Skuja, A. N. Streletsky, and A. B. Pakovich, *Solid State Commun.* **50**, 1069 (1984).
- ⁴⁶L. N. Skuja, A. R. Silin, and A. G. Boganov, *J. Non-Cryst. Solids* **63**, 431 (1984).
- ⁴⁷B. P. Gritsenko and V. M. Lisitsyn, *Sov. Phys. Solid State* **27**, 1330 (1985).
- ⁴⁸W. Hayes, M. J. Kane, O. Salminen, R. L. Wood, and S. P. Doherty, *J. Phys. C* **17**, 2943 (1984).
- ⁴⁹E. J. Friebele, D. L. Griscom, and M. J. Marrone, *J. Non-Cryst. Solids* **71**, 133 (1985).
- ⁵⁰M. Guzzi, M. Martini, M. Mattaini, F. Pio, and G. Spenolo, *Phys. Rev. B* **35**, 9407 (1987).
- ⁵¹P. W. Wang, R. F. Hagland, D. L. Kinser, M. H. Mendenhall, T. H. Tolk, and R. A. Weeks, *J. Non-Cryst. Solids* **102**, 288 (1988).
- ⁵²C. Itoh, K. Tanimura, and N. Itoh, *J. Phys. C* **21**, 4693 (1988).
- ⁵³R. Tohmon, Y. Shimogaichi, H. Mizuno, Y. Ohki, K. Nagasawa, and Y. Hama, *Phys. Rev. Lett.* **62**, 1388 (1989).
- ⁵⁴L. N. Skuja and A. N. Trukhin, *Phys. Rev. B* **39**, 3909 (1989).
- ⁵⁵C. Itoh, T. Suzuki, and N. Itoh, *Phys. Rev. B* **41**, 3794 (1990).
- ⁵⁶K. Awazu and H. Kawazoe, *J. Appl. Phys.* **68**, 3584 (1990).
- ⁵⁷T. Munekuni, Y. Yamanaka, Y. Shimogaichi, R. Tohmon, Y. Ohki, K. Nagasawa, and Y. Hama, *J. Appl. Phys.* **68**, 1212 (1990).
- ⁵⁸B. J. Luff and P. D. Townsend, *J. Phys. Condens. Matter* **2**, 8289 (1990).
- ⁵⁹H. Nishikawa, Y. Shiroyama, R. Nakamura, Y. Ohki, K. Nagasawa, and Y. Hama, *Phys. Rev. B* **45**(2), 586 (1992).
- ⁶⁰T. Hashimoto, S. Sakaue, H. Aoki, and M. Ichino, *Radiat. Measurements* **23**, 293 (1994), and references therein.
- ⁶¹M. O'Keeffe and B. G. Hyde, *Acta Crystallogr.* **34**, 27 (1978).
- ⁶²J. C. Brice, *Rev. Mod. Phys.* **57**, 105 (1985).
- ⁶³M. A. Stevens Kalceff and M. R. Phillips, *J. Appl. Phys.* **77**(8), 4125 (1995).
- ⁶⁴M. G. Jani, L. E. Halliburton, and E. E. Kohnke, *J. Appl. Phys.* **54**, 6321 (1983).
- ⁶⁵L. E. Halliburton, B. D. Perlson, R. A. Weeks, J. A. Weil, and M. C. Wintersgill, *Solid State Commun.* **30**, 575 (1979).
- ⁶⁶J. H. Stathis and M. A. Kastner, *Phys. Rev. B* **29**, 7079 (1984).
- ⁶⁷A. Kats, *Philips Res. Rep.* **17**, 133 (1962); **17**, 201 (1962).
- ⁶⁸R. Tohmon, A. Ikeda, Y. Shimogaichi, S. Munekuni, Y. Ohki, K. Nagasawa, and Y. Hama, *J. Appl. Phys.* **67**, 1302 (1990).
- ⁶⁹T. D. S. Hamilton, I. H. Munro, and G. Walker, in *Luminescence Spectroscopy*, edited by M. D. Lumb (Academic, London, 1978), Chap. 3.
- ⁷⁰M. O'Donoghue, *Quartz* (Butterworths, London, 1987).
- ⁷¹D. C. Joy (unpublished).
- ⁷²ORIGIN MicroCal Software, Inc., 22 Industrial Drive, E. Northhampton, MA 01060.
- ⁷³W. Kalceff (private communication).
- ⁷⁴J. Cazaux and C. Le Gressus, *Scan. Microsc.* **5**(1), 17 (1991).
- ⁷⁵M. N. Filippov (unpublished).
- ⁷⁶R. Castaing, Ph.D. thesis, Université de Paris, France, 1951.
- ⁷⁷M. R. Phillips, A. R. Moon, and M. A. Stevens Kalceff, *Microbeam Anal.* (to be published).
- ⁷⁸C. Kittel, *Introduction to Solid State Physics* (Wiley, New York, 1976).
- ⁷⁹J. Cazaux, *J. Appl. Phys.* **59**(5), 1418 (1986).
- ⁸⁰G. Blaise and C. Le Gressus, *J. Appl. Phys.* **69**, 6334 (1991).
- ⁸¹D. L. Griscom, *Phys. Rev. B* **20**, 1823 (1979).
- ⁸²P. Kaiser, *J. Opt. Soc. Am.* **64**, 475 (1974).
- ⁸³K. Tanimura, T. Tanaka, and N. Itoh, *Phys. Rev. Lett.* **51**, 423 (1983).
- ⁸⁴C. Itoh, K. Tanimura, N. Itoh, and M. Itoh, *Phys. Rev. B* **39**, 11 183 (1989).
- ⁸⁵K. Tanimura, C. Itoh, and N. Itoh, *J. Phys. C* **21**, 1869 (1988).
- ⁸⁶N. Itoh and K. Tanimura, *J. Phys. Chem. Solids* **51**, 717 (1990).
- ⁸⁷A. L. Shluger, *J. Phys. C* **21**, L431 (1988).
- ⁸⁸A. J. Fisher, W. Hayes, and A. M. Stoneham, *J. Chem. Soc. Faraday Trans. 2* **85**, 467 (1989).
- ⁸⁹Y. Bar-Yam, S. T. Pantelides, J. D. Joannopoulos, D. C. Allan, and M. P. Teter, *SiO₂ and Its Interfaces*, edited by S. T. Pantelides and G. Lucovsky, MRS Symposia Proceedings No. 105 (Materials Research Society, Pittsburgh, 1988), p. 223.
- ⁹⁰R. K. Brow, *J. Non-Cryst. Solids* **175**, 155 (1994).

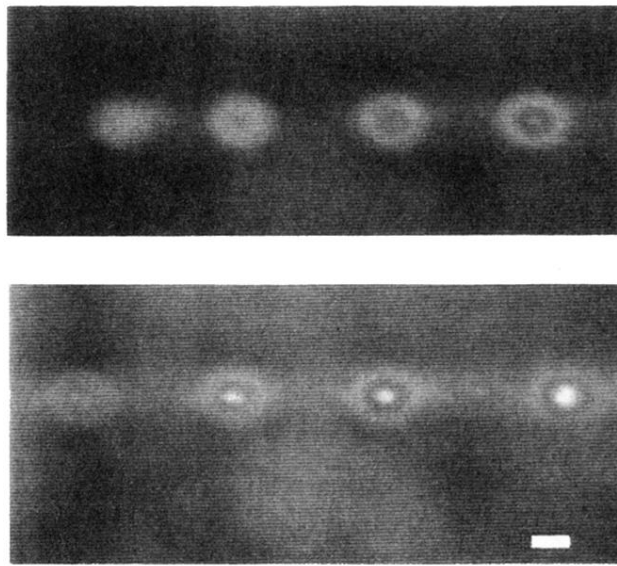


FIG. 8. Panchromatic CL micrograph of quartz previously irradiated with a normal focused stationary electron beam at 295 K for (top row, left to right) 15, 30, 45, 60 s and (second row, left to right) 75, 90, 105, and 200 s duration. The dimension marker is representative of 10 μm .